



*Imperial College London*

# IC Gabor Lens Project: Steady State Plasma Experiments

Ben Elliott

CID: 00952560

Supervisor: Dr. Piero Posocco

April 2017

# Acknowledgments

I would like to thank my supervisor, Dr. Piero Posocco, for his continuous assistance throughout the duration of the project, as well as my assessor, Dr. Jürgen Pozimski, for providing me with this opportunity.

I would also like to thank Chung Lim Cheung and Toby Nonnenmacher for working on this project alongside me and providing ongoing support.

## **Abstract:**

The aim of the investigation is to understand the factors that affect the nature of a plasma confined within a Gabor lens. The confinement conditions needed to sustain plasma in a Gabor lens operating at a voltage range of 8kV to 20kV and a current range from 14A to 27A have been investigated. The possible origins of instability, such as variation in pressure and temperature have been examined and improvements to the experimental setup suggested. It was found that an increase in temperature resulted in a decrease in discharge voltage, contrary to expectations from preliminary results. Data sets obtained at different vacuum pressures suggest that higher pressures restrict the voltage-current range over which a plasma can be confined. Fourier spectra of the plasma showed no evidence of significant instability over the recorded range. Future measurements should take steps to control temperature and investigate further the effect of pressure on the confinement conditions.

# Contents

<b>Introduction</b>	.	.	.	.	.	.	.	.	.	.	<b>5</b>
<b>Experimental Setup</b>	.	.	.	.	.	.	.	.	.	.	<b>6</b>
<b>Theory</b>	.	.	.	.	.	.	.	.	.	.	<b>7</b>
Confinement Conditions	.	.	.	.	.	.	.	.	.	.	7
Focussing Conditions	.	.	.	.	.	.	.	.	.	.	7
Paschen's Law	.	.	.	.	.	.	.	.	.	.	8
Charge Carrier Velocity Distribution	.	.	.	.	.	.	.	.	.	.	9
Discharge Regimes	.	.	.	.	.	.	.	.	.	.	9
Larmor Orbits	.	.	.	.	.	.	.	.	.	.	10
<b>Experimental Method</b>	.	.	.	.	.	.	.	.	.	.	<b>10</b>
Fourier Transform	.	.	.	.	.	.	.	.	.	.	10
Moving Detector	.	.	.	.	.	.	.	.	.	.	10
Fixed Voltage	.	.	.	.	.	.	.	.	.	.	11
<b>Results</b>	.	.	.	.	.	.	.	.	.	.	<b>11</b>
Preliminary Findings	.	.	.	.	.	.	.	.	.	.	11
Moving Detector	.	.	.	.	.	.	.	.	.	.	13
Fixed Voltage	.	.	.	.	.	.	.	.	.	.	14
Pressure Comparison	.	.	.	.	.	.	.	.	.	.	16
Temperature Comparison	.	.	.	.	.	.	.	.	.	.	17
Improvements	.	.	.	.	.	.	.	.	.	.	17
<b>Conclusion and Outlook</b>	.	.	.	.	.	.	.	.	.	.	<b>18</b>
<b>References</b>	.	.	.	.	.	.	.	.	.	.	<b>19</b>
<b>Appendices</b>	.	.	.	.	.	.	.	.	.	.	<b>20</b>

# Introduction

The Gabor lens is an axially symmetric space charge lens designed to focus charged particle beams through confinement of a non-neutral plasma.

The original design, proposed by Gabor in 1947 and displayed in figure 1 [1], used a magnetic field and electrical potential to confine electrons, thereby setting up a radial electric field used to focus positive ion beams. The magnetic field is produced using two coils in opposition. A hot cathode is placed at the point where the magnetic field-line crosses the axis of the lens. A cylindrical anode, with a high positive potential with respect to the cathode, is placed in the region where the magnetic field is homogeneous and axial. With the correct potential, the magnetic field prevents the electrons from reaching the anode. Electrodes with potential lower than the cathode are placed at both ends setting up a potential preventing the electrons from escaping longitudinally. The end result is a confined, homogeneous electron cloud.

The focussing of the ion beams aims to mitigate the effects of “beam blow-up”, a consequence of the positive ion charge of the beam. This effect applies to high-current ion beams and leads to an increase in the beam cross section due to radial motion of the ions resulting from the electric field of the space charge [2]. The high current ion beams require a high degree of space charge neutralisation, provided by a sea of negatively charged electrons, in order to propagate without degradation. The Gabor lens is advantageous in that it provides a mass independent focussing strength and operates on reduced electric and magnetic fields compared to conventional focussing devices [3].

Hadron therapy has recently emerged as an alternative to radiotherapy for the treatment of cancerous tumours. The current limiting factors for this treatment are the size and cost of the accelerators however, it has been suggested that an optical system such as the Gabor lens used in conjunction with a laser accelerated ion beam source can provide a cheaper and more compact solution. However, at present the particle distributions produced by such accelerators do not fulfil the medical requirements [4]. Further development and a more refined understanding of the focusing techniques employed by the Gabor lens could mean that laser accelerated ions become a possible form of cancer treatment [5].

The IC Gabor Lens was tested with a 1MeV  $H^+$  ion beam in 2015 at the Surrey on beam centre. The output beam formed ring shapes instead of focussed points with a correlation in the radius of the rings and the magnetic field. Results recorded from previous work using similar setups to the IC Gabor lens have shown that collective phenomena of the electron cloud can result in aberrations and emittance growth of the ion beam. Findings produced by Neuner [6] in 2000 displayed similar results however it was concluded that the hollow cylindrical form of the ion beams was due to high-current electron discharge, a feature not present in the IC Gabor lens setup. Despite these findings, there is no literature explaining the emergence of these rings.

The aim of this investigation is to explore the conditions needed to produce a stable electron cloud, without an ion beam, using the IC Gabor lens setup and to identify any possible causes of plasma instability.

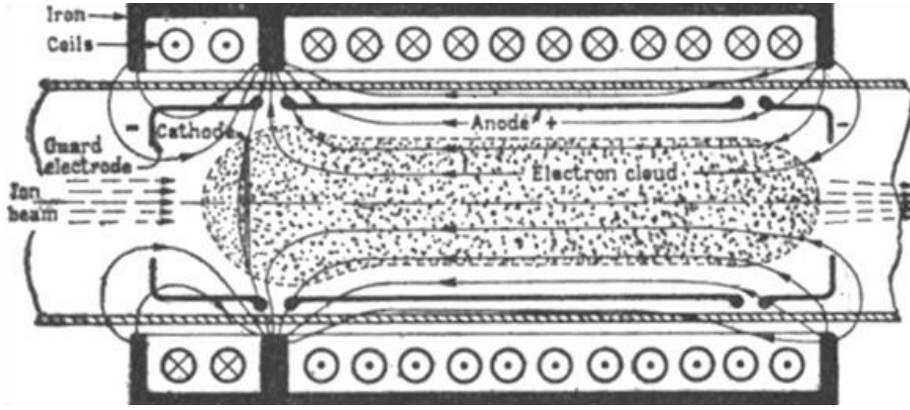


Figure 1: Design originally proposed by Gabor in 1947 for a space charge lens.

## Experimental Setup

The IC Gabor lens shown in figure 2 [7], differs from the design originally proposed by Gabor. Two concentric cylinders run the length of the lens with the inner cylinder held at a high voltage by a copper pin connected to an external high-voltage power supply. The outer cylinder is kept grounded so that a potential difference is set up between the two electrodes. A grounded copper electrode is located at each end of the lens acting as the guard electrodes to keep the electrons from escaping longitudinally. The magnetic field is provided by coils wrapped around the outer copper cylinder. As current is passed through these coils from an external source, a magnetic field in the axial direction is produced which confines the electrons radially. A vacuum tube contained within the lens is used to evacuate the cloud chamber to achieve pressures of the order  $10^{-6}/10^{-7}$  mbar.

Cosmic rays are used to ionise residual gas contained within the lens to release electrons from the outer shell of the atoms. The electrons then go on to further ionise the residual gas so that a self-sustaining plasma is produced. Due to the potential set up by the electric field, the electrons accelerate towards the electron chamber where they are confined axially and radially [8]. For the

purposes of this investigation, there was no need to pass an ion beam through the lens.

A detector, divided into 16 segments, is placed at one end of the lens in order to determine the nature of the confined plasma. As the charge carriers leave the lens via the detector, they induce a current and therefore a voltage on the detector which is displayed on a Tektronix DPO 3014 Digital Phosphor Oscilloscope. The segments can be wired so that any combination of segments corresponds to one of four channels on the oscilloscope.

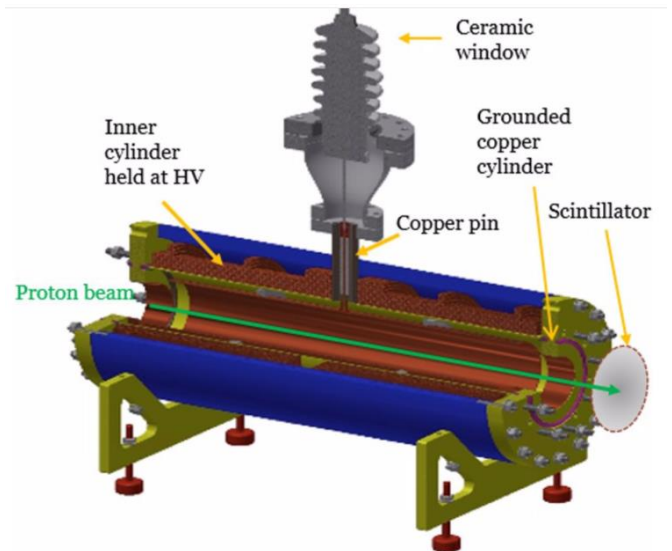


Figure 2: Schematic of the axially symmetric IC Gabor Lens with a proton beam passed through along its axis.

# Theory

## Confinement Conditions

Consider the equation of motion for the electron component of the plasma, ignoring ion motion:

$$m_e n_e \frac{dv}{dt} = -en_e(\mathbf{E} + \mathbf{v} \times \mathbf{B}) - \nabla p + \frac{en_e}{\sigma} \mathbf{j} \quad (1)$$

where  $p$  is the pressure of the electron component,  $\sigma$  is the plasma conductivity,  $\mathbf{j}$  is the current density of the beam and the other symbols all have their usual meaning. By making the assumption that the electrons are cold and the charge density of the beam is small compared to the electron density of the plasma, the final two terms of the right hand side of (1) can be neglected (as  $p = nk_b T$ ). Therefore, the condition for equilibrium is:

$$(\mathbf{E} + \mathbf{v} \times \mathbf{B}) = 0 \quad (2)$$

By taking the cross product of  $\mathbf{B}$  with (2), we can deduce that:

$$\mathbf{v}_\perp = \frac{(\mathbf{E} \times \mathbf{B})}{B^2} \quad (3)$$

which shows the  $\mathbf{E} \times \mathbf{B}$  drift. Considering a solenoidal field, the azimuthal component of the electric field will be zero as the electric field is perpendicular to the magnetic field. This implies that the magnetic flux tubes act as electric equipotential surfaces. Because of this effect, the two ground electrodes at either end of the lens act to fix the potential inside the lens.

The potential along the axis can be set to ground and then using Gauss's law and the azimuthal symmetry of the charge distribution it can be shown that the radial electric field,  $E_r$  varies with distance from the axis of the lens,  $r$ , as:

$$E_r = \frac{ne}{2\epsilon_0} \cdot r \quad (4)$$

where  $n$  is the uniform charge density. Integrating this to find the dependence of the electrostatic potential,  $\phi$ , with an electrode placed at radius  $R$  we find:

$$\phi = \phi_0 + \left(\frac{ne}{4\epsilon_0}\right) R^2 \quad (5)$$

where  $\phi_0$  is the potential on the axis [9].

## Focussing Conditions

The spatial charge density of the confined plasma determines the focal length of the lens. The charge density can be resolved into a radial and longitudinal component dependent on the transverse and longitudinal trapping conditions respectively. Gabor indicated that the transverse trapping condition, assuming an absence of external magnetic fields, is given by the Brillouin flow limit meaning that the maximum electron density can be calculated by:

$$n_{e,rad} = \frac{\epsilon_0}{2m_e} B_z^2 \quad (6)$$

where  $n_{e,rad}$  describes the maximum radial electron density and  $B_z$  represents the axial magnetic field.

Using equation (5), the space charge potential of a homogeneous electron cloud of radius  $r_A$  confined by an electrode potential  $V_A$  determines the maximum longitudinal electron density  $n_{e,l}$ :

$$n_{e,l} = \frac{4\epsilon_0 V_A}{er_A} \quad (7)$$

When the electrode is positively charged, the radial E-field will point towards the axis and the lens will focus positive ions.

Using equation (4) the single particle equation of motion can be obtained:

$$r'' + \frac{V_A}{UR^2} = 0 \quad (8)$$

where  $U$  is the accelerating potential of the ions and is equal to their kinetic energy divided by their charge. Solving the second order differential equation provides an expression for the focal length,  $f$ , of the lens given by:

$$\frac{1}{f} = \sqrt{K} \sin \sqrt{KL} \quad (9)$$

where  $K = V_A/UR^2$ , defined as the focussing constant, and  $L$  is the length of the lens, estimated by the distance between the two grounded electrodes [9].

By applying the thin lens approximation, the focal length of the Gabor lens can also be expressed as:

$$\frac{1}{f} = \frac{e}{8m_e} \frac{B_z^2}{U} L \quad (10)$$

The focal length of the lens can be used to determine the average electron density in the cloud chamber for a given ion beam energy. Using the short lens approximation and assuming a homogeneous space charge cloud the average electron density is given by:

$$\bar{n}_e = \frac{4\varepsilon_0 W_B}{f \cdot e} \cdot L \quad (11)$$

where  $W_B$  is the beam energy [3].

The radial and longitudinal filling factors,  $k_{\text{rad},l}$  describe the ratio of the average electron density to the radial or longitudinal electron density and describe the trapping efficiency of the lens.

$$k_{\text{rad},l} = \frac{\bar{n}_e}{n_{e,\text{rad},l}} \quad (12)$$

## Paschen's Law

Paschen's law states that the breakdown voltage, the voltage necessary to start a discharge, between two electrodes in a gas is a function of the product of the gap length and the pressure. A graph of the Paschen curve, displayed in figure 3 [10], shows that below a certain pressure for a given gap length, the voltage needed to start a discharge increases as the pressure is decreased. Above the curve minimum, the increase in breakdown voltage is almost linear with increasing pressure.

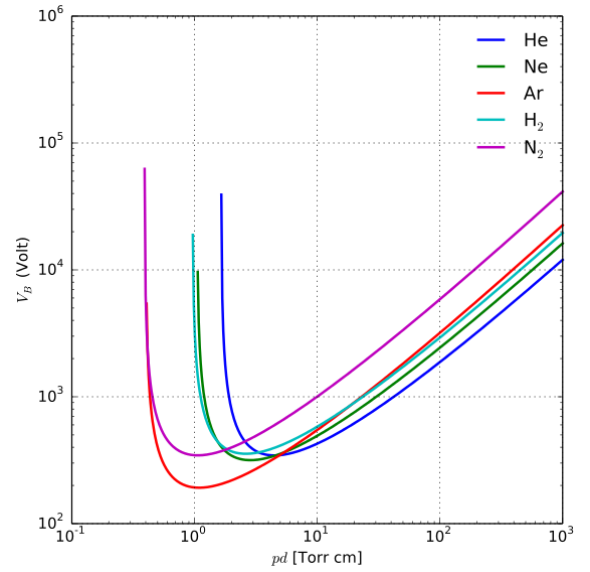


Figure 3: Paschen curves for helium, neon, argon, hydrogen and nitrogen

The breakdown voltage,  $V$ , is given by:

$$V = \frac{apd}{\ln(pd)+b} \quad (13)$$

where  $p$  is the pressure,  $d$  is the gap distance between electrodes, and the constants  $a$  and  $b$  depend on the composition of the gas, which ultimately determine both the minimum arc voltage and the distance at which it occurs.

In the absence of collisional ionisation, the gap length between the electrodes is equal to the geometrical distance between them. However due to the collisions with residual



gas molecules, and the presence of a magnetic field, the actual distance the electrons travel between electrodes will be much larger.

## Charge Carrier Velocity Distribution

The positively charged cylindrical anode sets up a potential so that the ions produced from the collisional ionisation travel out of the lens. The velocity of the charge carriers leaving the lens and hitting the detector can be resolved into two components, their radial velocity and their longitudinal velocity. The longitudinal velocity arises from the applied electrical potential and as the ions undergo further collisions on their journey out of the lens, they become thermalized meaning their longitudinal velocity forms a narrow distribution resembling that of a Gaussian.

The radial electric field sets up a potential gradient which the ions follow forming the origin of their radial velocity [11]. Due to the homogeneity of the electron cloud, the radial velocity of the ions form a rectangle function. Combining the two velocity components by convoluting their distributions produces a bell-shape distribution meaning it is expected that the majority of ions will leave the lens along its axis with a drop-off in ion number at larger radii.

## Discharge Regimes

Filling the lens with electrons can be achieved in three ways [12]. Colliding beam ions with the residual gas, producing electrons from a hot cathode or producing electrons via a gas discharge. For the purposes of this setup, the electrons are produced via a gas discharge, the conditions for which require a low vacuum pressure. Electrons move from areas of electron

density higher than the radial trapping limit to lower density areas meaning that a homogeneous electron distribution forms from an inhomogeneous electron production.

Once the conditions needed to sustain and confine a plasma within the lens are satisfied, the nature of the plasma can be controlled by altering the voltage on the high voltage (HV) power supply or the current supplied to the coils. For a certain base voltage supplied by the HV supply, there is a range of current under which a plasma will be produced in the voltage controlled regime. In this regime, the cylindrical anode and the ground electrode are not connected and the discharge current observed on the HV supply is of the order  $\sim 0.1\text{mA}$ .

Beyond this current range, the plasma enters the current controlled regime where the anode and grounded electrode connect via electron flow. In this regime, a value for the potential drop required to confine the electrons can no longer be defined. An increase in the pressure is observed and the discharge current becomes significant.

The HV supply acts as a potential divider distributing voltage between the anode and an internal resistance. In the voltage controlled regime the anode receives all the voltage provided by the HV supply as the internal resistance is negligible and the potential drop between the anode and the ground electrode is well defined. Once the current regime is entered, the electrons are expelled to the anode and the current passing through the HV supply becomes significant therefore increasing the internal resistance.

For a steady state plasma, the rate of electron production is equal to the rate of electron expulsion with the majority of the electrons confined within the chamber. There is no collective movement of the plasma, such

as a plasma oscillation/rotation in the steady state. The ions also leave the chamber as fast as they are produced leading to a stable internal pressure.

## Larmor Orbits

For a magnetic field in a given direction, a charged particle will experience a force resulting in a circular orbit of the particle in a plane perpendicular to the B-field. The angular frequency of this motion is the Larmor frequency,  $\Omega$ , and is given by:

$$\Omega = \frac{qB}{m} \quad (14)$$

Where  $q$  and  $m$  are the charge and mass of the charged particle respectively and  $B$  is the strength of the magnetic field. The radius of this resulting orbit,  $r_L$ , follows from the kinematics of circular motion and can be calculated from:

$$r_L = \frac{v_{\perp}}{\Omega} \quad (15)$$

where  $v_{\perp}$  is the velocity component of the particle perpendicular to the magnetic field [13].

## Experimental Method

### Fourier Transform

The detector, pictured in figure 4, was wired to the oscilloscope via a junction box such that each segment at a given radius corresponded to one channel displayed on the oscilloscope (see figure 5). A sample of the output voltage of each channel was recorded at a sample rate of  $2.5 \times 10^7$  samples per second for a time of 4 milliseconds.

Using a short code generated via the program Anaconda, a Fourier spectrum, ranging from 0 to 12.5MHz, of the output signal was produced as well as a plot of the offset voltage

as a function of time. This method was repeated for varying lens parameters both with and without confinement of a plasma.



Figure 4: Image of the segmented detector centred at the end of the IC Gabor lens cloud chamber.

## Moving Detector

The detector is mounted on a rail such that it can be moved across a range of 75mm in a direction transverse to axis of the lens. The voltage of the anode and current supplied to the coils contained within the lens were adjusted so that a plasma was confined within the lens under the voltage controlled regime. The detector was then shifted across the full range of its movement with the voltage produced from each channel recorded every 2mm. This measurement was taken with the detector wired in a radial arrangement and then repeated in a sector arrangement, also depicted in figure 5.

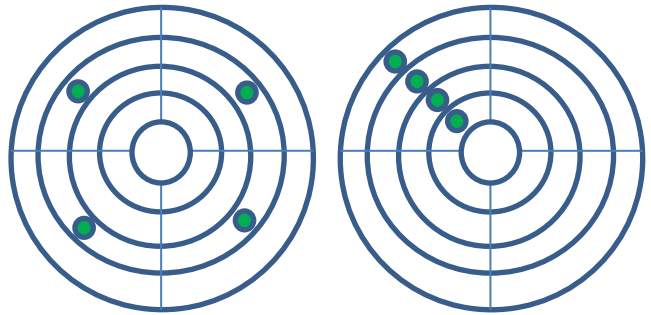


Figure 5: Diagrammatic depiction of the radial arrangement (left) and the sector arrangement (right) where the highlighted segments correspond to a channel on the oscilloscope.

# Fixed Voltage

For a given voltage supplied to the anode by the HV supply, the current provided to the coils was varied until a plasma was detected within the lens. The voltage for each channel on the oscilloscope was recorded as the current was increased in increments of 0.1A until the current regime was entered, at which point no further data was taken. These measurements were taken with the detector wired in the radial arrangement and were repeated over a range of base voltages from 8kV-20kV and at varying pressures.

## Results

### Preliminary Findings

From preliminary measurements of the frequency spectrum of the signal produced in the lens, both with and without a plasma, it was noted that there was little difference between the spectrum with a plasma burning and the spectrum without. These measurements were taken with the detector wired in the radial arrangement with the innermost radius corresponding to channel 1 and the outermost radius to channel 4. The purpose of these results was to provide a clearer picture of how to proceed with the investigation.

Figure 6 shows the Fourier spectrum of the signal received from the detector at a pressure of  $3.46 \times 10^{-7}$  mbar with neither the power supply nor the current supply turned on. This reading was taken in order to gain an idea of the background noise produced by the unionised residual gas contained within the chamber or by any other sources.

It was expected that an instability in the plasma would produce a significant peak representing a plasma oscillation frequency

on the Fourier spectrum when burning a plasma.

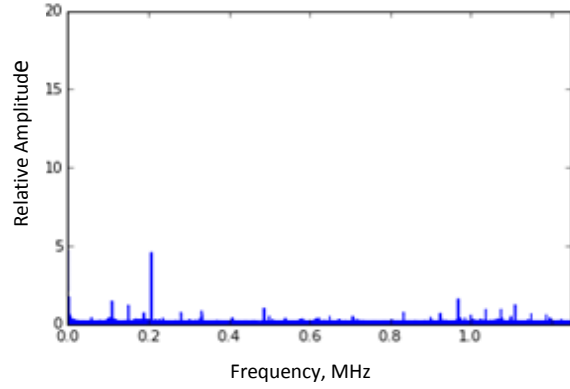


Figure 6: Fourier spectrum of the signal received from channel 1 with nothing turned on.

No significant peak is expected to appear on the spectrum if the plasma is in a perfectly stable state. To ensure that the background noise would not overpower any signal we expected to see as a result of the plasma, a makeshift Faraday cage was constructed and the junction box connecting the detector to the oscilloscope was placed inside to reduce any ‘antenna’ effects of the connecting wires. The Fourier transform was then retaken at the same pressure as before and is displayed in figure 7. The spectrum in figure 7 does show some noise reduction when compared to figure 6.

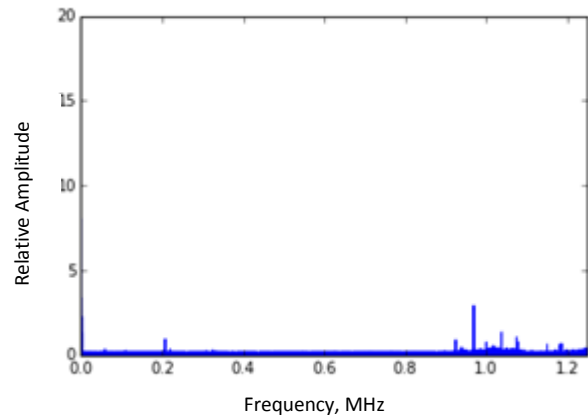


Figure 7: Fourier spectrum of the signal received from channel 1 with nothing turned on and the junction box placed in the Faraday cage.

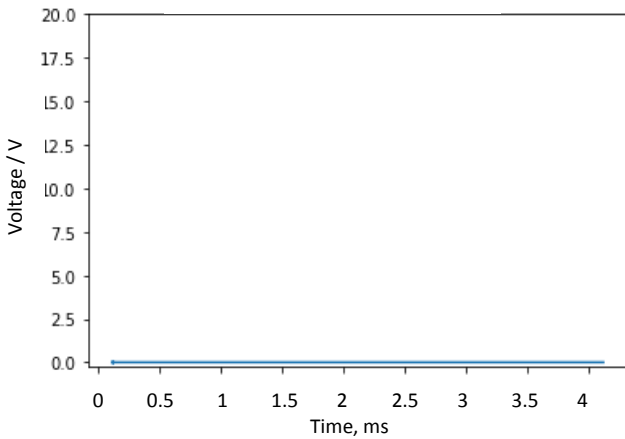
With the box placed in the Faraday cage, still no significant peaks were observed on the spectra when burning a plasma. One possibility is that the recorded frequency range is too narrow, and a frequency corresponding to an instability may be present at higher frequencies.

The offset voltage as a function of time was recorded for a number of different plasma conditions, examples of which are given in figure 8. As expected no offset voltage is observed when there is no plasma in the lens, as described by figure 8a.

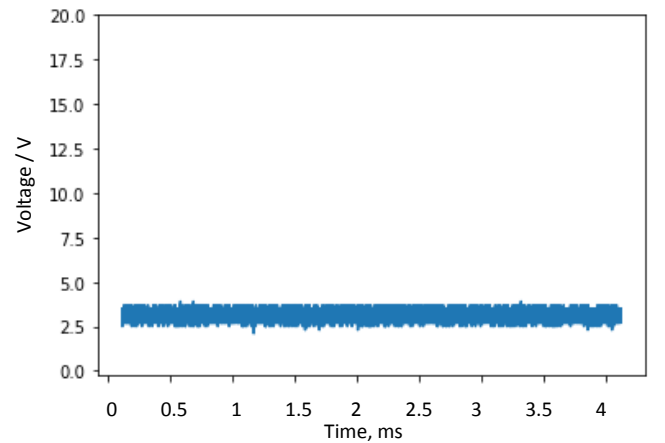
Figure 8b shows the offset voltage when producing a plasma in the voltage controlled regime. In this case, a distinctive offset voltage of approximately 3V is observed due to the discharge of positively charged ions hitting the detector. The offset voltage shows

a well-defined width, an indication that a discharge of only one charge carrier type is observed, as the electrons are well confined within the cloud chamber.

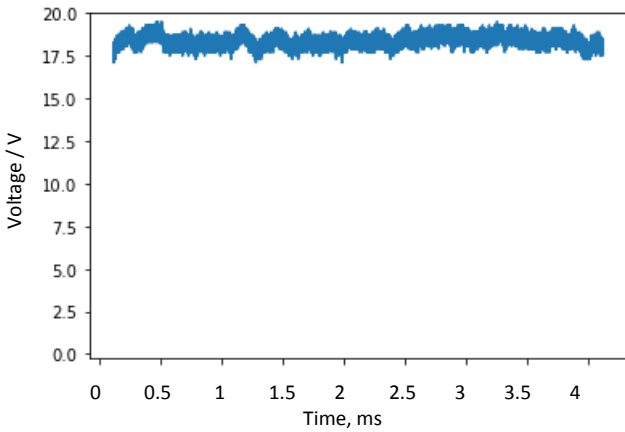
The current passing through the coils was increased to a point where the current regime was entered and the pressure increased by a factor of approximately 10 from  $1.62 \times 10^{-6} \text{ mbar}$  to  $2.95 \times 10^{-5} \text{ mbar}$ . In this case the magnitude of the magnetic field determines the radial confinement conditions for the electron cloud. According to equation (6), a larger magnetic field results in a larger radial electron density. The space charge density of the plasma increases until the potential becomes larger than the magnetic potential confining it. Electrons in the plasma are released both radially and longitudinally until the space charge density



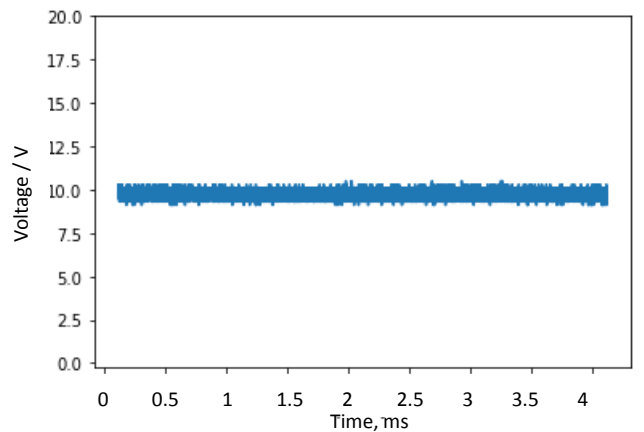
a) No Plasma



b) Voltage Regime



c) Current Regime



d) Current limited

Figure 8: Voltage offset amplitude as a function of time for a) no plasma b) voltage controlled plasma c) current controlled plasma d) current limited plasma

returns to a value low enough for confinement, however the continued production of electrons means the electron cloud needs to continuously expel electrons in an attempt to return to equilibrium. The rise in pressure is a result of the increased number of collisional events occurring as the electrons travel to the anode. The voltage offset shown in figure 8c displays a much higher amplitude than that in 8b with a varying width over time, displaying clearly this effect. The offset oscillates over time as the contribution from the longitudinally expelled electrons is observed.

The plasma was then brought into the current limited regime by increasing the discharge current on the HV supply. The decrease in internal resistance results in a larger voltage supplied to the anode restoring the required electron confinement conditions. The voltage offset for this case, displayed in figure 8d, was lower than that of the current controlled plasma but higher than that of a voltage controlled plasma under the same conditions. The pressure was seen to be  $8.25 \times 10^{-6}$  mbar. The higher voltage offset and pressure is a result of the increased number of residual ions contained within the lens after entering the current regime.

It was noted that increasing the scaling factor on the oscilloscope appeared to increase both the width and the amplitude of the voltage offset band observed. An increase in the width of the band is expected as the resolution is increased however the resolution of the oscilloscope has no effect on the internal workings of the lens and so the average amplitude of the band should remain constant for all resolutions. It was concluded that the increasing amplitude was a result of thermal effects resultant from an increase in

the temperature of the equipment as current is continually passed through the coils.

## Moving Detector

As mentioned in the theory section, the expected ion velocity distribution resembles a bell shape function. With the detector wired in the radial arrangement, the corresponding radius of each channel determines the observed distribution. For a stable plasma under the conditions of a 15kV electrode potential, 20A supplied to the coils and a pressure of  $7.74 \times 10^{-7}$  mbar, the bell-shape was observed across channel 1, corresponding to the innermost radius, with an inverse bell shape observed across the other 3 channels.

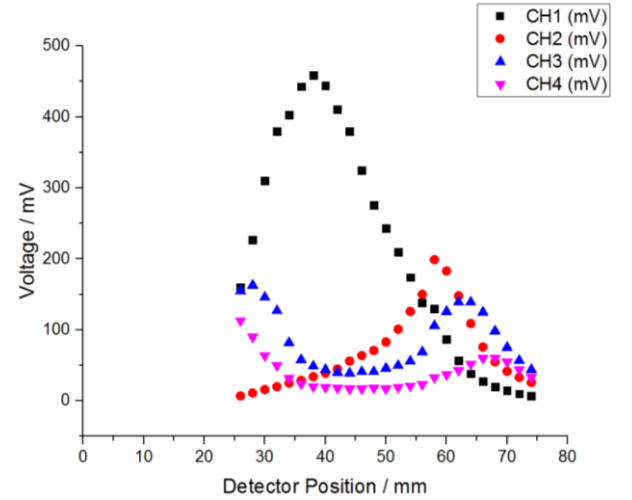


Figure 9: The voltage measured for each channel as a function of the position of the detector (radial arrangement) with a plasma burning at 15kV, 20A, and  $7.74 \times 10^{-7}$  mbar.

In this case, the radius of channel 1 is smaller than the radius of the cone produced by the ion velocity distribution under these plasma conditions and the radii of channels 2, 3 and 4 are larger than the bell curve radius. If the radius of the channel is smaller than the radius of the velocity bell curve, the detector receives all the discharging ions and shows a bell shape profile. If the radius of the channel is larger than the radius of the

velocity bell curve, the detector would not receive any ions at the centre. As the detector shifts to the right (left), the left (right) side of the radial segment will be moved into the ion discharge cone and will begin to produce a voltage signal, producing an inverted bell shape distribution. The radius of the velocity cone is determined by the strength of the magnetic field. A larger magnetic field results in a stronger confinement, and so, a smaller cone radius.

At all detector positions below 28mm, a large discharge occurs and no data can be taken as the voltage across all 4 channels rapidly rises. This effect could be due to electrical contact between the detector and the lens. The asymmetry displayed by channels 2 and 4 indicated an issue with the internal wiring of the detector. Through the use of a multimeter, it was discovered that some segments were unintentionally grounded and so the detector was removed from the lens and rewired.

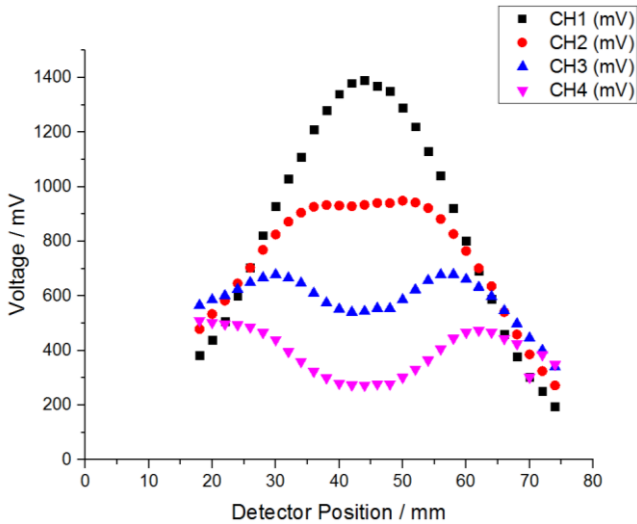


Figure 10: Voltage as a function of the position of the detector (radial arrangement) after rewiring the detector with a plasma burning at 10kV, 20A, and  $1.8 \times 10^{-8}$  mbar.

The data was retaken for similar plasma conditions, as shown in figure 10. All 4 channels displayed a symmetry across the range of movement, matching the expected

result. Figure 10 was compared with theoretical predictions produced by a code that calculates the radius of the velocity distribution cone as a function of the magnetic field within the lens. The profile of figure 11 matches the profile of a cone radius of  $\sim 15$ mm.

The measurements were repeated after the detector had been fixed with the detector wired in the sector arrangement. The expected result for a perfectly centred detector is symmetric about the midpoint with all 4 peaks having the same magnitude. Prior to these results, displayed in figure 11, it was known that the detector was shifted downwards slightly, explaining the difference in magnitude of channels 2 and 3. However the similar magnitudes of channels 1 and 4 and the small offset between the peaks suggest that the detector is tilted on its diagonal axis.

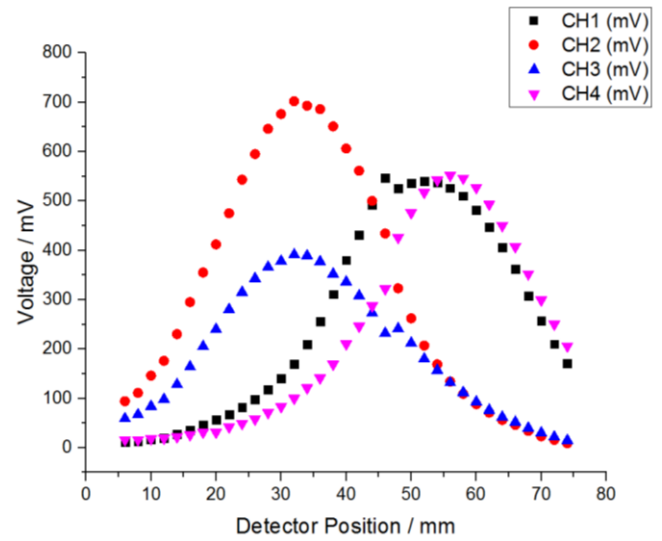


Figure 11: The voltage measured for each channel as a function of the position of the detector (sector arrangement) after rewiring the detector with a plasma burning at 10kV, 20A, and  $7.07 \times 10^{-7}$  mbar.

## Fixed Voltage

The purpose of these results was to determine under which conditions a stable plasma is produced and how varying the



parameters affects the stability of the plasma. Given the previous discovery that the temperature of the equipment affects the voltage measured at the detector, the equipment was allowed to cool between subsequent sets of measurements.

An example of the dependence of the voltage measured at the detector on the current supplied to the magnetic field is given in figure 12 for a base voltage of 10kV. The profile of the plot is similar for all base voltage values (see appendix A).

In this example, for the lower current values (16A - 19A) small peaks in the voltage are observed. These peaks correspond to failed attempts to produce a self-sustaining plasma as the Gabor conditions are not satisfied. The sharp rise in voltage at  $\sim 19$ A represents the production of a plasma in the voltage controlled regime.

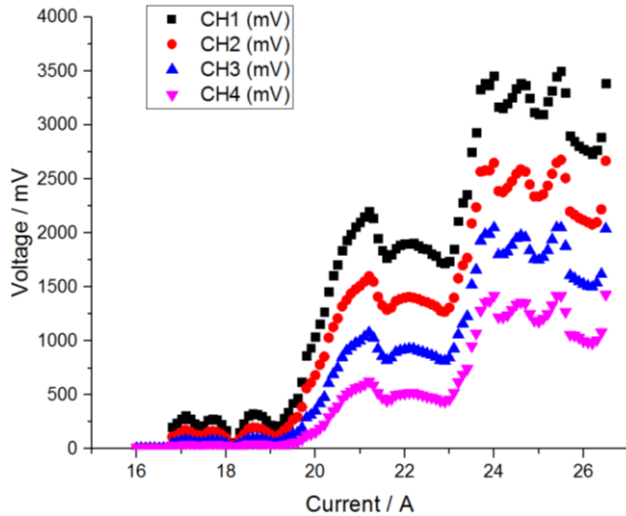


Figure 12: Base voltage 10kV, initial pressure  $6.05 \times 10^{-7}$ mbar, initial temperature  $29.2^\circ\text{C}$ .

As the current supplied to the coils, and therefore the strength of the magnetic field, is increased, the number of collisional ionisation events increases and so an increase in measured voltage with increasing current is expected. The plot displays two plateau regions however, where the measured voltage remains approximately

constant over a small range of current. In these regions, the contribution from the longitudinal expulsion of electrons lowers the measured voltage. The voltage contribution from the ions continues to increase, however the discharged electrons offset the ion contribution so that the measured voltage over these regions remains approximately constant.

The second plateau region oscillates more intensely than the first. This is due to the same effect described previously explaining the oscillation in the voltage offset plots. As the current is increased further a large discharge is observed as the space charge density overcomes the confinement potentials and no more data is taken.

A table describing the current range over which a plasma burning in the voltage controlled regime is observed for each base voltage is given below. The initial pressures over which the data was taken ranged from  $6.05 \times 10^{-7}$ mbar –  $8.06 \times 10^{-7}$ mbar. No correlation between the base voltage on the HV supply and the current at which we first observe a stable plasma was apparent (see appendix B). There is also no correlation between base voltage and the current value at which the current regime is entered.

Base Voltage (kV)	Current Range Lower Pressure (A)	Current Range Higher Pressure (A)
8	17.4 - 24.5	16.5 – 18.1
10	16.7 – 26.5	16.4 – 19.5
12	14.8 – 27.6	14.5 – 18.6
14	15.9 – 23.9	15.8 – 19.3
16	16.8 – 25.5	16.6 – 18.8
20	16.7 – 22.1	16.6 – 18.7

Table 1: Current range over which a plasma is produced in the voltage controlled regime for a given base voltage for a pressure  $\sim 10^{-7}$ mbar and  $\sim 10^{-6}$ mbar.

For a base voltage of 12kV, a set of measurements were taken after entering the

current controlled regime. After falling into the current limited regime, the discharge current of the HV supply was increased in increments of 0.01mA and the voltage measured at the detector recorded for each value. The current supplied to the coils was kept constant at 27A across the range of measurements, and the pressure after the discharge was  $1.61 \times 10^{-6}$  mbar.

From figure 13, it can be seen that the voltage measured at the detector increased almost linearly with the HV discharge current, implying that a larger number of ions are expelled longitudinally as the current is increased, or a fewer number of electrons are. It was also noted that upon entering the current regime, the voltage between the anode and electrode dropped to 7kV and rose back to the pre-set value of 12kV as the discharge current was increased.

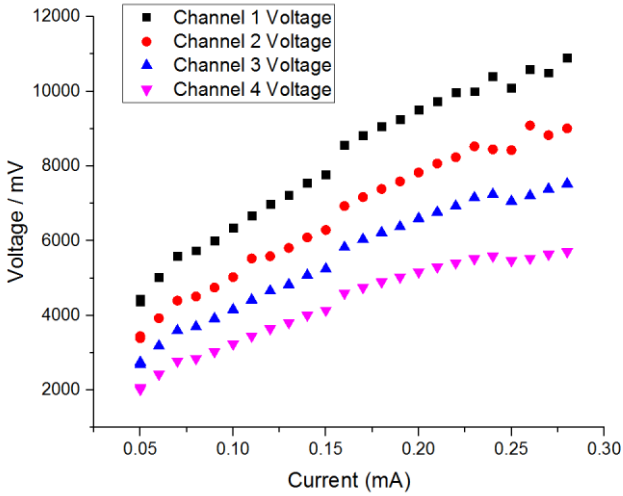


Figure 13: Measured voltage as a function of the variable discharge current supplied in the current limited regime.

As previously mentioned, the HV supply acts as a potential divider. As the discharge current is increased, the effective resistance between the anode and the ground electrode decreases and more ions remain in the lens. The electrons travel to the walls of the lens and are able to ionise the surface of the wall,

meaning there is more residual gas ions contained within the lens.

This effect accounts for the rise in pressure observed and the potential between the anode and electrode rises, restoring the confinement conditions for the electrons. This results in a decrease in the number of electrons escaping the lens and therefore an increase in the number of ionisation events, seen as an increase in measured voltage.

## Pressure Comparison

The measurements taken across the base voltages were repeated at higher pressure values. The initial pressure range for these measurements was  $3.19 \times 10^{-6}$  mbar –  $3.57 \times 10^{-6}$  mbar.

At the higher pressures, only one plateau region was observed before the current regime was entered. The current range over which data was taken, also shown in table 1, is significantly smaller at the higher pressure. The initial current at which a plasma is observed remains fairly constant between the two pressures however. This suggests a relationship between the confinement conditions for the electron cloud and the vacuum pressure.

As the magnetic field strength is increased for each base voltage value, the radius of the plasma decreases and the number of collisions that the electrons undergo as they escape radially increases. This increases the path length of the electrons on their journey to the anode, as their mean free path is decreased. For each base voltage, an increase in the magnetic field, and therefore the path length, resulted in an electric discharge between the anode and the electrode meaning that as the path length is increased, the breakdown voltage decreases. With reference to figure 3, this means that for the



pressures used in the investigation, the Gabor lens is operating in the negative gradient region of the Paschen curve. Estimations of the magnitude of the path length require a more extensive knowledge of the plasma itself, the likes of which can be determined through the use of an optical spectrometer.

## Temperature Comparison

To explore further the effects of the temperature of the equipment on the measurements, two data sets were collected at a base voltage of 20kV with initial temperatures of 22.2 °C and 38.6 °C. The pressure was kept as constant as possible across the two data sets. As shown in figure 14, the measurement taken at the higher temperature consistently measured a lower voltage, contrary to expectations from the preliminary results.

The scattering of the electrons with ions occurs as a result of the Coloumb force between the ion and the electron and the time interval over which the electron remains within the influence of the ion. Electrons with a higher velocity are less collisional, as their time interval within the ions influence is shorter. At higher temperatures, the electrons will have more kinetic energy, meaning that less collisional ionisation events will occur within the lens resulting in a lower voltage measured at the detector. However, the temperature difference between the two data sets (16.4K) is negligible when comared to the estimated electron temperature of ~100eV and so this phenomena does not explain the observed results.

Further investigation into the nature of the plama is needed to provide an explanation for these results.

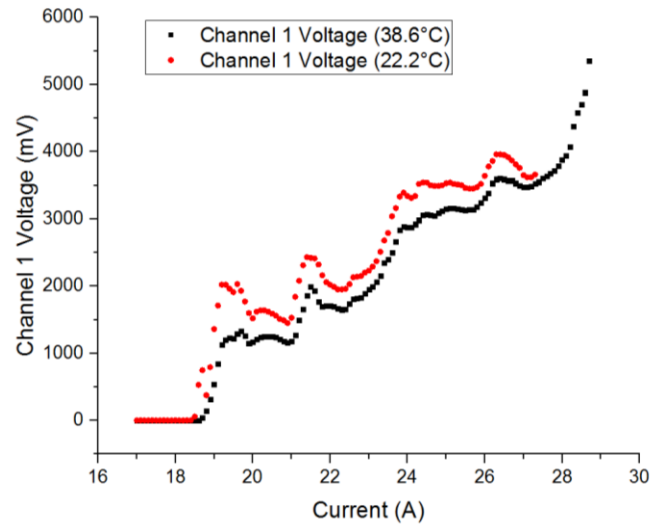


Figure 14: Measured voltage as a function of current at 20kV for starting temperatures of 38.6 °C and 22.2 °C.

## Improvements

An optical spectrometer can provide a greater insight into the composition of the plasma as well as providing more accurate estimations of the variables such as the electron temperature. With knowledge of the exact components of the plasma, the region of the Paschen curve over which the lens operates can be determined more rigorously and precise predications of the breakdown voltage can be made.

As seen from the results, the temperature of the equipment has an effect on the outcome of the experiment. Ideally, temperature should remain a controlled variable for the purposes of this experiment and so the installation of a cooling system would further progress the investigation. The use of an optical spectrometer will also aid in determining the nature in which the temperature affects the composition of the plasma, if at all.

Analysis of Fourier spectra taken over a larger frequency range may also reveal as of yet unobserved instabilities. It is possible that significant peaks were missed due to a narrow frequency range.

## Conclusion and Outlook

The aim of this investigation was to understand the factors that affect the nature of a plasma confined within the IC Gabor lens. No significant peaks thought to correspond to a plasma oscillation frequency were observed on the Fourier spectra taken over the frequency range of 0MHz-12.5MHz. For future investigations, sampling for longer timer periods may show evidence of instabilities. Under the plasma conditions imposed within this investigation, a confined plasma of radius  $\sim 15\text{mm}$  was produced and confirmed through comparison between experimental observations and theoretical predictions. The base voltage measurements, produced plateau regions, where stronger confinement conditions resulted in a constant voltage output, an indication of the longitudinal expulsion of electrons.

Whilst the influence of pressure and temperature on the plasma were briefly explored, the exact effect these factors have on the nature of the plasma requires further investigation and a more in depth analysis of the composition of the plasma, provided through the use of an optical spectrometer.

## References:

- [1] – D. Gabor, 1947. *A Space-Charge Lens for the Focusing Of Ion Beams*. Nature, 160(4053), pp.89-90.
- [2] – A. Goncharov, 2013. *Invited Review Article: The Electrostatic Plasma Lens*. Review of scientific instruments, 84.
- [3] - O. Meusel, M. Droba, B. Glaeser, K. Schulte. *Experimental Studies of Stable Confined Electron Clouds Using Gabor Lenses*. IAP, University Frankfurt/Main, Germany.
- [4] – J.K. Pozimski, M. Aslaninejad, P.A. Posocco, 2013. *Advanced Gabor Lens Lattice for Medical Applications*, Imperial College, London.
- [5] - J. Pozimski, M. Aslaninejad, 2013. *Gabor Lenses for Capture and Energy Selection of Laser Driven Ion Beams in Cancer Treatment*. Imperial College, London.
- [6] – U. Neuner, R. Bock, M. Roth, P. Spiller, C. Constantin, U.N. Funk, M. Geissel, S. Hakuli, D.H.H Hoffmann, J. Jacoby, A. Kozyreva, 2000. *Shaping of Intense Ion Beams into Hollow Cylindrical Form*. Physical review letters, 85(21), p.4518.
- [7] - P. A. Posocco, J. K. Pozimski, Y. Xia, M. Merchant, 2016. *First Test of the Imperial College Gabor (Plasma) Lens Prototype at the Surrey Ion Beam Centre*, Imperial College, London.
- [8] – Y. Xia, 2016. *The IC Gabor Lens Project: Analysis of the Data Collected During the 2015 Experimental Campaign*, Imperial College, London.
- [9] - J .A.Palkovic, R.Hrcn, G. Lee, F.E.Mills, C.W. Schmidt, J.Wendt, D.E.Young, 1988. *Measurements on a Gabor Lens for Neutralizing and Focusing a 30 KeV Proton Beam*, University of Wisconsin, Madison.
- [10] – W.S. Boyle, P. Kisliuk, 1955. *Departure from Paschen's Law of Breakdown in Gases*, SciTech Connect Vol 97.
- [11] - C. Davis, 1984. *Ion motion and emission profiles in low-pressure cylindrical discharges*, Physical Review A Vol 32, No. 6, Electrical Engineering Department, University of Maryland,
- [12] - J.Pozimski, P.Grol3, R.Diilling and T.Weis, *First Experimental Studies of a Gabor-Plasma-Lens in Frankfurt*. Institut fiir Angewandte Physik der Johann Wolfgang Goethe-Universittit
- [13] - S. Lebedev, 2016. *Plasma Physics 3<sup>rd</sup> Year Lecture Notes*. Blackett Laboratory, Imperial College, London.

# Appendices

## Appendix A

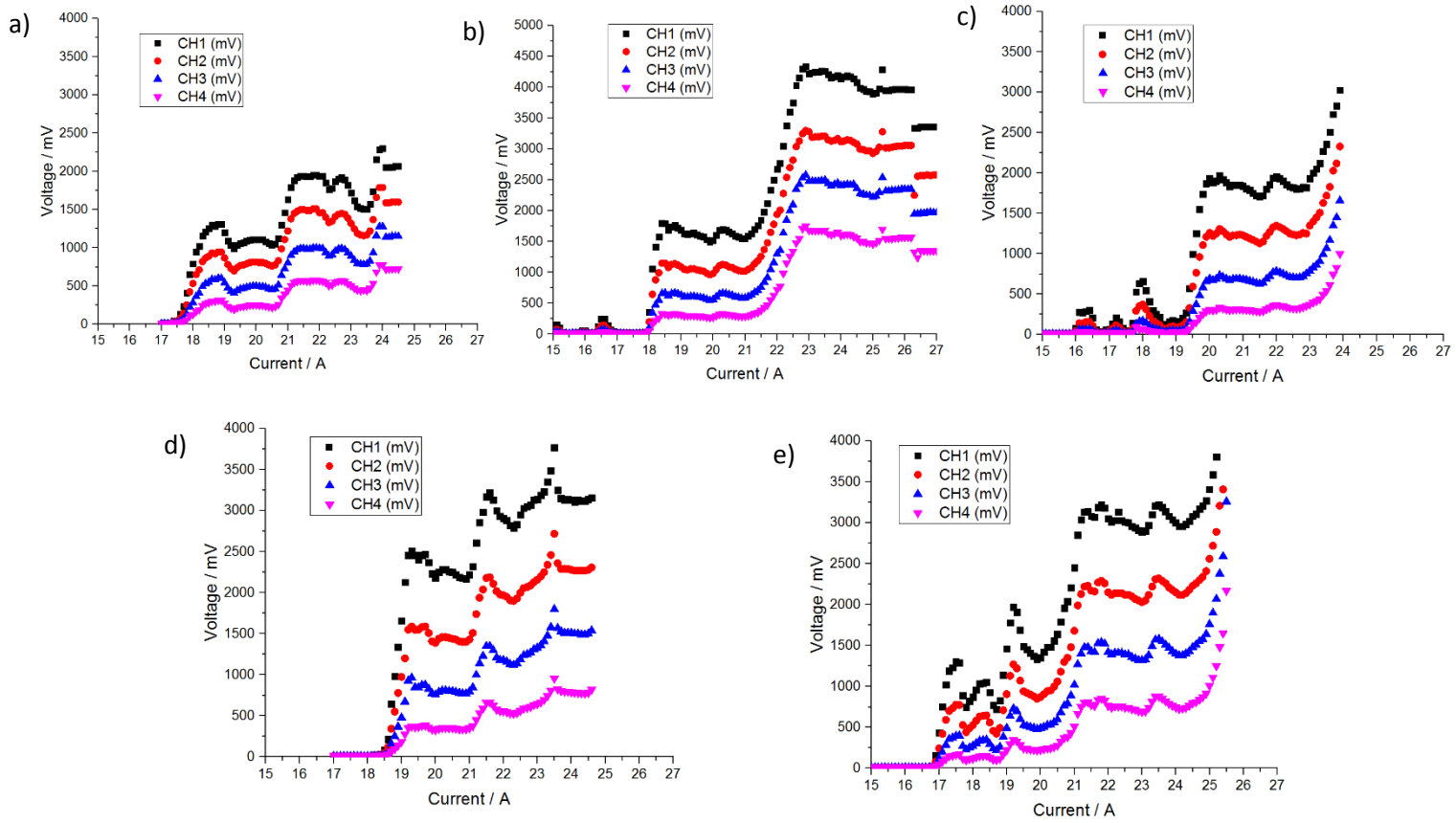


Figure 15: a) Base voltage 8kV initial pressure  $7.11 \times 10^{-7}$  mbar initial temperature 31.2°C. b) 12kV,  $8.06 \times 10^{-7}$  mbar, 25.7°C. c) 14kV,  $6.36 \times 10^{-7}$  mbar, 29.9°C. d) 16kV,  $6.36 \times 10^{-7}$  mbar, 21.2°C. e) 20kV,  $6.69 \times 10^{-7}$  mbar, 29.3°C.

## Appendix B

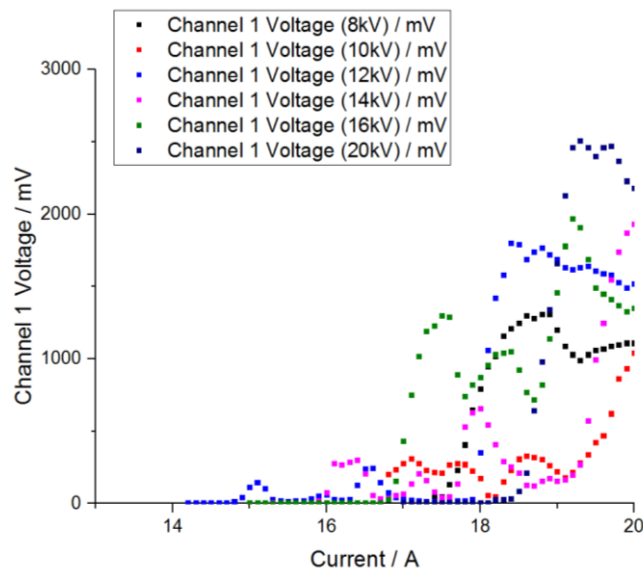


Figure 16: A comparison between each base voltage and the current value at which we observe a plasma in the voltage controlled regime